

Flow Characteristics Simulation Using CFD on Semi-Submersible Platforms

AG.MALLIKARJUNA, Associate Professor & Head of H&S Dept., St.Johns College of Engineering and Technology, Yemmiganur, Kurnool(Dist.). E_mail Id: mallipraveena1023@gmail.com.

S VEERA REDDY, Associate Professor & Head of H&S Dept., St.Johns College of Engineering and Technology, Yemmiganur, Kurnool(Dist.) E_mail Id: veerakuppagallu@gmail.com

Abstract: The turbulent flow around a semi-submersible platform is simulated in this work using Ansys Fluent. The computational domain is shaped as a rectangular horizontal canal, with the semi-submersible platform positioned within. No slip boundary conditions are applied to the channel's top, bottom, left, and right walls. The velocity input and pressure outlet boundary conditions are provided for the front and rear walls. Two pontoons, four square columns, and two bracings comprise the semi-submersible platform. The issue is represented as three-dimensional, transient, incompressible flow, with turbulence represented using the Large eddy simulation (LES) turbulence model. The computational domain has 4,72,749 hexahedral mesh cells. The Reynolds number (Re) in the range of 104 Re 106, as well as the geometry of the columns, are varied in the parametric analysis. Plotting stream function, velocity, and pressure contours is used to conduct the inquiry. We saw vortex shedding and flow separation between the semi-submersible platform's front and rear columns. The strength of flow separation rises as the Reynolds number increases. By showing the coefficients of lift and drag for various Reynolds numbers and column forms, the transient flow features of the lift and drag forces are analysed..

Keywords: *CFD, LES turbulence model, Reynolds number, Semi-submersible platform.*

I. INTRODUCTION

Semi-submersible platforms are among the most common offshore structures used for oil and gas exploration in the sea. Semi-submersibles often operate in a variety of difficult circumstances within the sea, necessitating an entire study of the flow characteristics of a semi-submersible. In this study, we use ANSYS Fluent to investigate the flow characteristics of a four-column semi-submersible platform while accounting for turbulent flow around the platform. The parametric study approach is carried out by altering the Reynolds number (Re) in the range of 104 Re 106 as well as the shape of the columns. Drag and lift forces are important in the operation of the semi-submersible. As a result, we are also analysing the semi-lift submersible's and drag in this research. Liu et al. [1] conducted an outstanding investigation to determine the flow features distributed among four square-shaped cylinders arranged in a square pattern. For the parametric study, they considered spacing ratios and array attack angles and discovered that both the drag and lift forces experienced around the cylindrical columns show a very small difference for different L/D values, with the fluctuating forces reaching their maximum when the L/D value equals 4.14. The article also demonstrates that lift force peaks for downstream cylinders at an angle of $= 15^\circ$. Goncalves et al. [2] studied the Vortex Induced Motion (VIM) of a four square column semi-submersible. They ran several model studies to assess the effect of hull appendages and different headings. The final findings include information regarding different movements such as in-line, transverse, and yaw motions, as well as combined motions in the XY plane and a study of both drag and lift forces. They determined that

vortex-induced transverse motion exists only at decreased velocity levels ranging from 4.0 to 14.0. The greatest transverse amplitude occurs about 40% of the column width, at incidence angles of 30° and 45°. They also confirmed that the biggest yaw motion occurred at 0° incidence and that the highest amplitudes emerged at 45° incidence. Ma et al. [3] investigate the structure dynamic reactions under short-term sea conditions with both wind and load. They ultimately discovered a link between wind and waves. They discovered a link between wind speed and wave height using the Mixture Simulation approach, and they then enlarged the Wave Scatter Diagram and time series of wind/wave pressure across the platform translated using Workbench-AQWA. Holland et al. [4] studied the transverse forces caused by vortex shedding with current velocities in the Gulf of Mexico using a full scale CFD analysis. They confirm that the helical strakes included in the geometry serve to end the coherence of the vortex shedding and quantitatively examine their performance. The research notes that the four column configuration without pontoons and yaw movements at 0° angle and 45° angle of incidences showed the most significant transverse reactions to the maximum of fluctuating lift forces caused by the well-established.

Pitch motion and nonlinear effects of heave motion on pitch restoring coefficient are all addressed mathematically by Wei et al. [6]. To explore the coupled motion characteristics and validate the mathematical model, they used numerical simulations and several standard wave tests. In order to evaluate the mathematical model's capacity to forecast motion instability and accurately replicate nonlinear phenomena, they observed a unique pitch-motion profile and a double-period event. Motion instability was explored using a validated and tested model, and ways to mitigate it were advised. An improved mathematical model built on potential theory is proposed under irregular wave conditions to simulate a semi-submersible platform's response to motion, and the results show that the nonlinear hydrostatic effect of bracings increases resonance frequency as motion amplitude increases (Tian et al. [7])

According to Sharma et al, the design of a semi-submersible vehicle, the design of a perfect substitute for a specified operating depth, and all designing measures have been discussed in detail. It also includes an overview of the motion and structural attachments of semi-submersibles, as well as a review of current contributions in the industrial and academic domains to the development of column stabilised semi-submersible hulls for deep water operations. A boundary element method for both frequency and time domains was employed by Ghafari et al. [10] to investigate the dynamic responses of floating platforms in the second-order Stokes incident wave, and the results accurately show that as platforms come closer together, diffraction force, motions and mooring line tension for the semi-submersible platform decrease. In addition, they found that when the wave length increased, the movements of the semi-submersible platform increased as well..

II. MATHEMATICAL MODELLING AND NUMERICAL METHOD

During this investigation, the computational domain is 15 m long, 10 m wide, and 10 m in height. Inlet wall is 5 m away, and the semi-submersible measures 1.32 m in length, 0.81 m broad, and 0.48 m height. The domain's entrance and outflow are its front and rear faces, while its four fixed walls are its top, bottom, left, and right. A turbulent water flow model is used in the numerical simulations, which are done using Ansys Fluent. To simulate turbulent flow for velocity fields, the Reynolds Averaged Navier-Stokes (RANS) equation is used as a starting point. The kinetic energy and dissipation rate of turbulence are studied using the Large eddy simulation (LES) turbulence model. The time averaged governing equations are as follows:

$$\frac{\partial \bar{u}_i}{\partial t} + \frac{\partial \bar{u}_i}{\partial x_j} = 0 \quad (1)$$

$$\frac{\partial \bar{u}_i}{\partial t} + j u_i \frac{\partial \bar{u}_i}{\partial x_j} - \bar{\rho} \frac{\partial p}{\partial x} + \dots \quad (2)$$

$$\frac{\partial k}{\partial t} + i u_x \frac{\partial k}{\partial x} - \frac{\partial}{\partial x_j} \left[\frac{\mu}{\sigma} \frac{\partial u_i}{\partial x_j} \right] + \dots \quad (3)$$

$$\frac{\partial \varepsilon}{\partial t} + i u_x \frac{\partial \varepsilon}{\partial x} - \frac{\partial}{\partial x_j} \left[\frac{\mu}{\sigma} \frac{\partial u_i}{\partial x_j} \right] + \dots \quad (4)$$

Kinetic and dissipative fields are represented by the asterisk (*) and the fluid density is represented by the asterisk (*). To figure out how much a body is being lifted by a fluid, one may use

$$F_l = 1/2 \cdot C_l \cdot \rho \cdot v^2 \cdot A \quad (5)$$

'The lifting force is represented by 'Fl,' the lifting coefficient by 'Cl,' the fluid density by ', ' the flow velocity by 'v,' and the body area by 'A.'

$$F_d = 1/2 \cdot C_d \cdot \rho \cdot v^2 \cdot A \quad (6)$$

"Cl" is the drag coefficient, "" is the fluid density, "v" is the flow velocity, and "A" is the surface area of the body.

Coupled algorithm is used to link pressure and velocity in simulations. Second-order pressure and momentum are second-order upwind in the spatial discretization of gradient. An implicit transient formulation of the second order is used.

III. RESULTS AND DISCUSSION

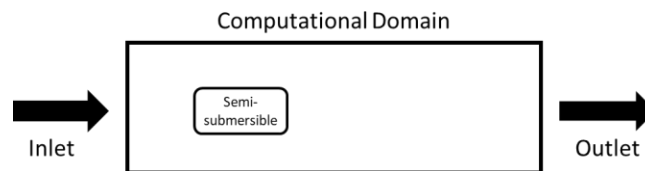


Fig. 1. Schematic diagram of the setup

An illustration of fluid flow is shown in Figure 1. By altering the Reynolds number, we are able to simulate the flow in the computational domain in the range of $Re = 104 - Re = 106$. Vortex shedding and flow separation have been detected around where the semi-submersible is now submerged. Changing the intake velocity alters the Reynolds number. We examine three distinct scenarios in this research.

As a result of varying the velocity of the input, we can determine the flow characteristics at these three different speeds. In each of these scenarios, we show the velocity streamlines, velocity contours, and pressure contours visually to help visualise the data. The charts of lift and drag coefficients are also presented.

Table – I: Reynolds number values corresponding to inlet velocities

Sl No	Inlet Velocity (m/s)	Reynolds Number (Re)
1	0.1	5.58×10^4
2	5	2.79×10^6
3	10	5.58×10^6

A table shows the Reynolds numbers for each of the three inlet velocity scenarios.

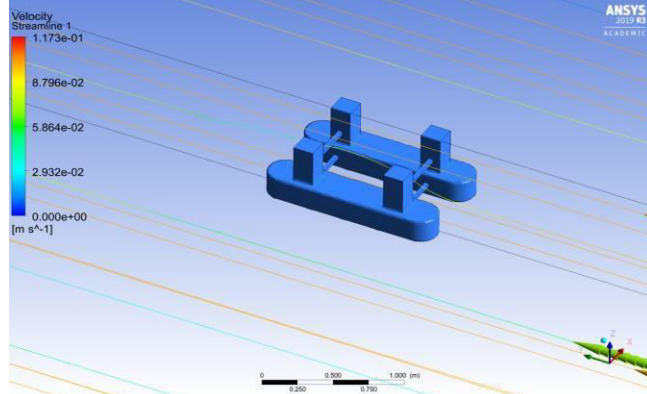


Fig. 2. (a). Velocity streamlines when $v = 0.1$ m/s

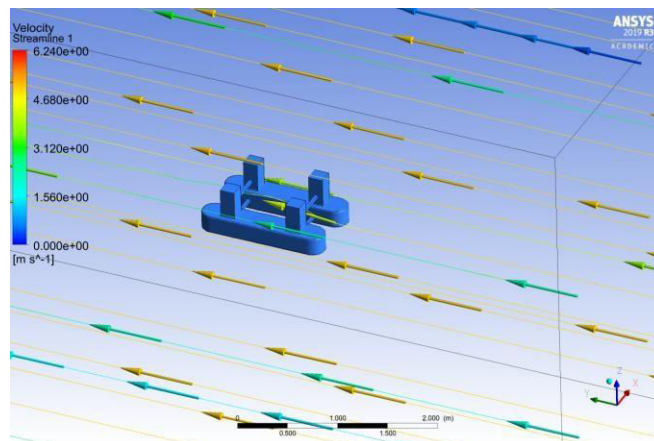


Fig. 2. (b). Velocity streamlines when $v = 5$ m/s

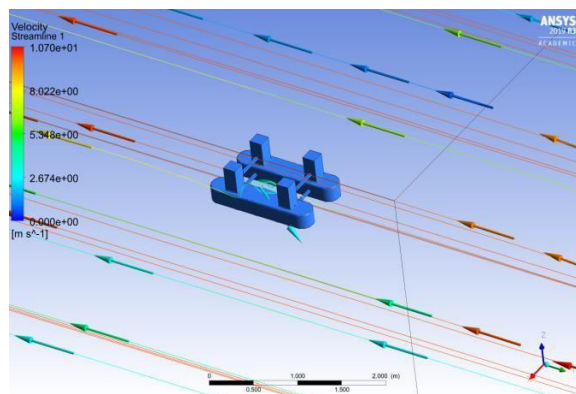


Fig. 2. (c). Velocity Streamlines when $v = 10$ m/s

For each of the three intake velocity scenarios, the streamlines are shown in Figures 2(a), 2(b), and 2(c). As the speed of the semi-submersible rises, so does the flow around and inside of it. The semi-central submersible's axis is exhibiting a strange route for the flow of air. As the inflow velocity rises, the pattern gets more erratic. At 10 m/s, the streamline between the pontoons in Fig. 2. (c) takes on a swirling pattern, indicating the shedding of vortices. When a semi-submersible is travelling at a high velocity, vortex shedding occurs between the two pontoons of the vessel.

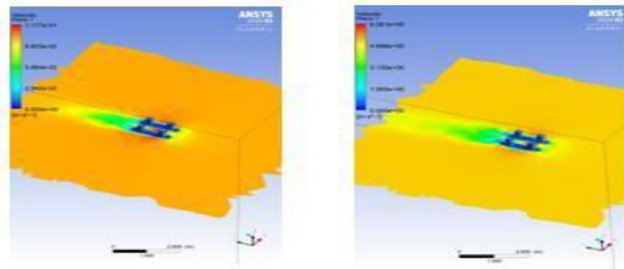
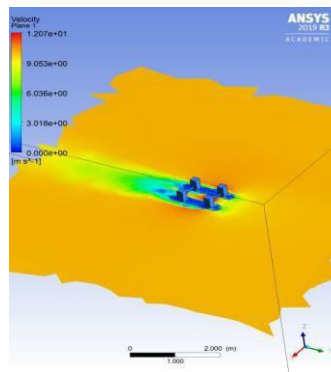


Fig. 3. (a). Velocity contour **Fig. 3. (b). Velocity contour**

when $v = 0.1$ m/s

when $v = 5$ m/s

Fig. 3. (c). Velocity contour when $v = 10$ m/s



A plane perpendicular to the pontoons is seen in Figs. 3 (a), (b), and (c). The maximum velocity is seen near the centre of the vortex, suggesting shedding of the vortex. The use of various colours clearly illustrates flow separation. The flow separation distance grows in direct proportion to the inflow velocity. Compared to the other two situations, the flow reunites at a more distant site in the highest-velocity scenario.

We can observe that the pattern continues to intensify as the input velocity increases. Pressure contours exhibit the same problem. They, too, are following the same general direction. This pattern of pressure contours is repeated in each occurrence with an increased value. In Fig. 4, (a), (b), and (c), pressure contours are shown.

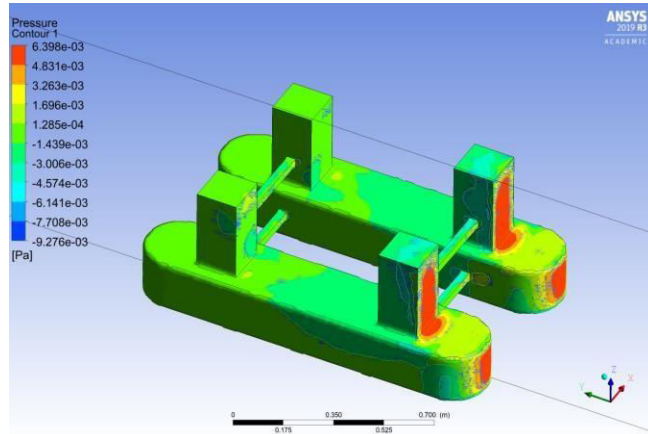


Fig. 4. (a). Pressure contour when $v = 0.1$ m/s

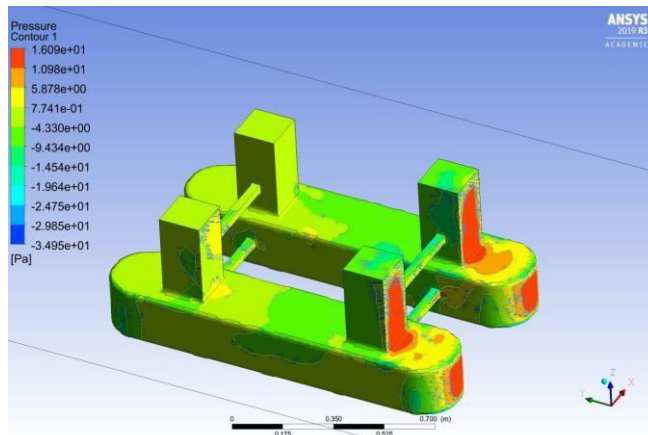


Fig. 4. (b). Pressure contour when $v = 5$ m/s

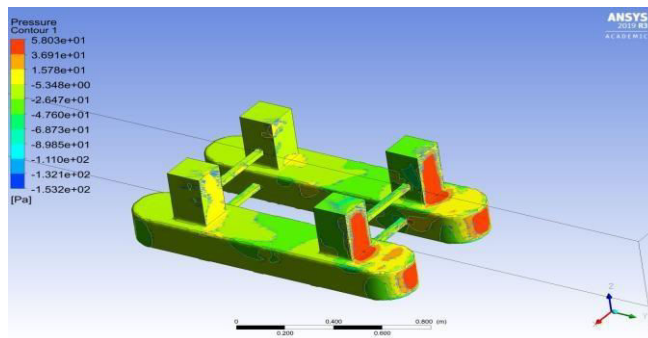
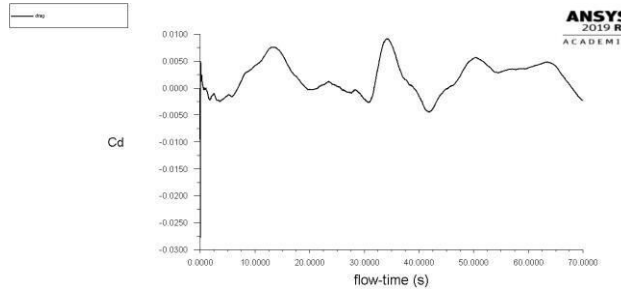


Fig. 4. (c). Pressure contour when $v = 10$ m/s

The semi-submersible is subjected to a large amount of lift and drag. Lift and drag coefficients were shown graphically (Cl flow-time graph of (Cd, and Cd). As a result, we were able to determine the relationship between entrance velocity and lift and drag coefficients.

Figure 5 (a) depicts the drag coefficient (Cd) vs flow time at an input velocity of 0.1 m/s. Between 0.010 and 0.005, Cd reaches its highest and lowest values in this time period. Figure 5. (b) shows a Cd value range of 0.0020 to -0.0015. When the inflow velocity is 5 m/s, this occurs.. However, there are a lot more variations



in this scenario than in the preceding one. The same pattern can be observed in Fig. 5 with a velocity of 10 m/s (c). Fluctuations may be seen often. There are two extremes in the range of Cd's value: 0.0025 and - 0.0025.

Fig. 5. (a). Coefficient of drag vs flow-time when $v = 0.1$ m/s

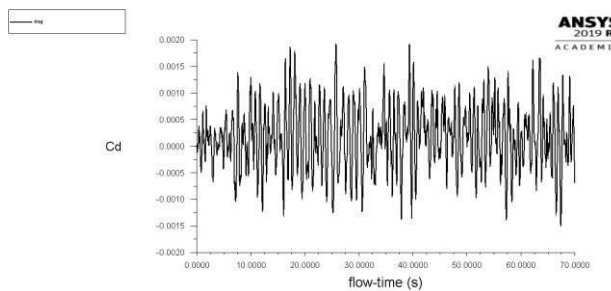


Fig. 5. (b). Coefficient of drag vs flow-time when $v = 5$ m/s

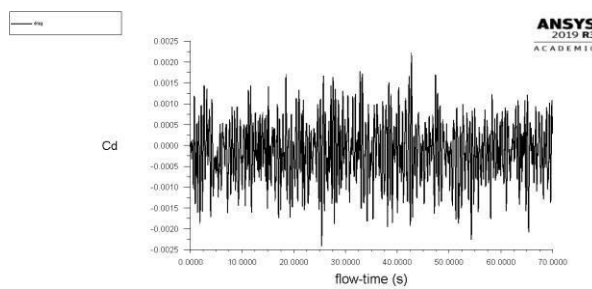


Fig. 5. (c). Coefficient of drag vs flow-time when $v = 10$ m/s

The graph becomes increasingly erratic as the velocity rises. For the overall flow-time, we take the average and Cd in the third scenario comes out on top. As a result, we may conclude that the drag force rises as the input velocity increases.

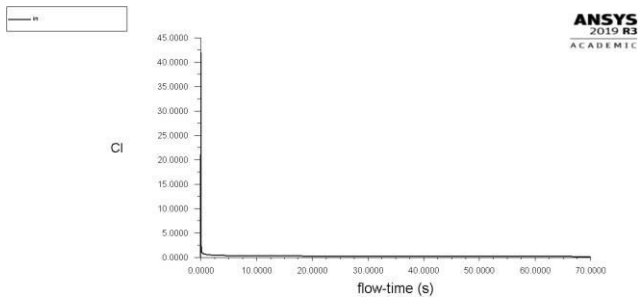


Fig. 6. (a). Coefficient of lift vs flow-time when $v = 0.1$ m/s

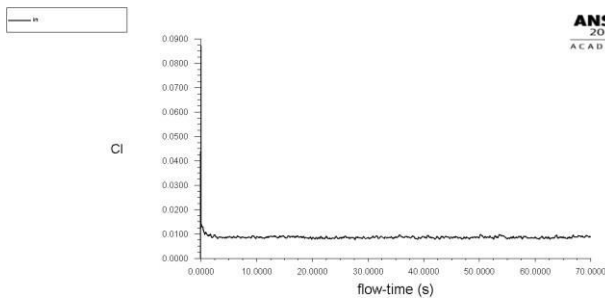


Fig. 6. (b). Coefficient of lift vs flow-time when $v = 5$ m/s

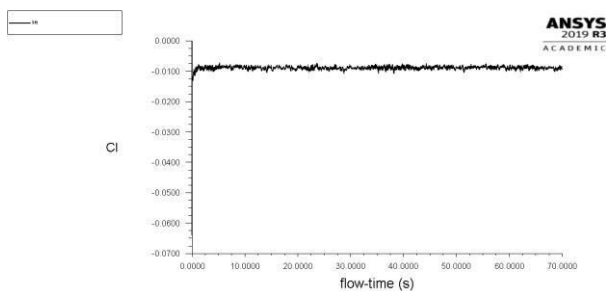


Fig. 6. (c). Coefficient of lift vs flow-time when $v = 10$ m/s

When the input velocity is 0.1 m/s, 5 m/s, and 10 m/s, respectively, Fig. 6. (a), Fig. 6. (b), and Fig. 6. (c) show the coefficient of lift (Cl). Semi-submersibles experience no lift force when intake velocity is less than 1 m/s, which is why Cl values are almost nil. The Cl value is 0.0100 in Fig. 6. (b). The axis of velocity was flipped in the third instance. As a result, in Figure 6, Cl has a negative value (c). When it comes to the graph, it is identical to the second example, except there are more fluctuations. As a result, the spread in the mean Cl values in these two scenarios is rather modest. Changing the inflow velocity does not have a substantial effect on the lift force or lift coefficient. We employed a pressure-based solution for all three simulations. The flow is transitory and the development of absolute velocity is taken into account. Large Eddy Simulation (LES) turbulence has been engaged and the sub-grid size model employed is WALE. In this case, we'll use a pressure-velocity coupling model. Gradients, pressure, and momentum are all constrained by central differencing in spatial discretization. The implicit transient formulation of second order has been selected.

ONCLUSION

The turbulent flow around a semi-submerged platform in a computational domain is studied numerically. Large Eddy Simulation (LES) turbulence model is used in the computational fluid

dynamics (CFD) technique to describe the turbulent flow. Different entrance velocities are studied and the stream line patterns, velocity contours, and pressure contours are examined for comparison and analysis. Vortex shedding occurs near the centre of the semi-submersible and increases in intensity as the inlet velocity rises. These movements are influenced by the columns, pontoons, and bracings. The flow-time is displayed against the coefficients of lift and drag experienced by the semi-submersible. Although the input velocity has a significant impact on the coefficient of drag (C_d), it has little influence on the coefficient of lift (C_l). An effective semi-submersible platform and the best place for it to be used in offshore applications will be aided by this study's findings.

REFERENCES

1. M. Liu, L. Xiao and L. Yang, Experimental investigation of flow characteristics around four square-cylinder arrays at subcritical Reynolds numbers, *International Journal of Naval Architecture Ocean Engineering* (2015), PP.7:906~919
2. R.T. Goncalves, G.F. Rosetti, A.L.C. Fajarra, A.C. Oliveira, Experimental study on vortex-induced motions of a semi-submersible platform with four square columns, Part I: Effects of current incidence angle and hull appendages, *Ocean Engineering* (2012), PP.150~169
3. J. Ma, D. Zhou, Z. Han, K. Zhang, Y. Bao, L. Dong, Fluctuating wind and wave simulations and its application structural analysis of a semi-submersible offshore platform, *International Journal of Naval Architecture and Ocean Engineering* (2019), PP.624~637
4. V. Holland, T. Tezdogan*, E. Oguz, Full-scale CFD investigations of helical strakes as a means of reducing the vortex induced forces on a semi-submersible, *Ocean Engineering* 137 (2017), PP.338~351
5. L. Xiao, M. Liu, Y. Liang, L. Tao, Experimental and numerical studies of the pontoon effect on vortex-induced motions of deep-draft semi-submersibles, *Journal of Fluids and Structures* 72 (2017), PP.59~79
6. H. Wei, L. Xiao, X. Tian, Y.M. Low, Nonlinear coupling and instability of heave, roll and pitch motions of semi-submersibles with bracings, *Journal of Fluids and Structures* 83 (2018), PP.171~193
7. X. Tian, H. Wei, L. Xiao, Ying Min Low, M. Liu, Effects of bracings and motion coupling on resonance features of semi-submersible platform under irregular wave conditions, *Journal of Fluids and Structures* 92 (2020), PP.102~783
8. R. Sharma, T.W. Kim, O.P. Sha and S.C. Misra, Issues in offshore platform research - Part 1: Semi-submersibles, *International Journal of Naval Architecture and Ocean Engineering* (2010), PP.2:155~170
9. A.C. Odijie, F. Wang, J. Ye, A review of floating submersible hull systems: Column stabilized unit, *Ocean Engineering* 144(2017), PP.191~202
10. H.R. Ghafari, M.J. Ketabdari, H. Ghassemi, E. Homayoun, Numerical study on the hydrodynamic interaction between two floating platforms in Caspian Sea environmental conditions, *Ocean Engineering* 188 (2019), PP.106~273